Molecular Simulation of Strain Dependence of Vibrational Frequencies for Montmorillonite Clay and Analysis of Strain Transfer in a Polymer−Clay Nanocomposite

Amrit Kalra,[†] David M. Parks,[‡] and Gregory C. Rutledge*[,†]

Department of Chemical Engineering and Department of Mechanical Engineering, Massachusetts Institute of Technology, Cambridge, Massachusetts 02139

Received September 15, 2006; Revised Manuscript Received October 20, 2006

ABSTRACT: Molecular dynamics simulations are used to determine the vibrational density of states for a model montmorillonite clay as well as the spectral shifts with applied strain for significant peaks in the 1000−1300 cm^{-1} range. Under uniaxial deformation with fixed lateral dimensions, the spectral shifts are found to be around −29 and −40 cm^{-1}/% strain in the clay, with little dependence on direction of applied strain within the plane of the clay platelet. Using Eshelby's method, a strain transfer efficiency of 5.6% is predicted for the nanocomposite with 5 wt % exfoliated clay. This results in a predicted spectral shift of −1.6 to −2.2 cm^{-1}/% macrostrain in the nanocomposite, in reasonable agreement with the experimental results of Loo and Gleason (*Macromolecules* **2003**, *36*, 2587).

Introduction

The advent of nanocomposites formed by blending polymers with inorganic clay has resulted in many exciting applications in aircraft, food packaging, and automobile industries. One of the most widely used formulations is montmorillonite clay (MMT) blended in nylon-6, which exhibits enhanced mechanical properties such as increases in elastic modulus, yield strength, and heat distortion temperature.[1,2] Many studies have highlighted such property enhancements even at very low loading of clay fillers (typically around 5%) (ref 3 and references therein). When fully exfoliated within the polymer matrix, the clay particles form thin platelets with a thickness of 1 nm or less and a high aspect ratio of 10−1000. As a result, an efficient load transfer from the polymer matrix to dispersed clay particles is expected. Transfer of load from the polymer matrix to the clay particles depends additionally on a variety of factors such as strength of polymer−clay interactions, clay orientation, degree of dispersion, etc. Sheng et al. recently reported the results of a multiscale micromechanical finite element model that relates the overall mechanical properties of polymer−clay nanocomposites to those of the polymer matrix and of the dispersed clay particles, accounting for the several effects of polymer matrix modulus, clay modulus, clay loading, degree of exfoliation, and clay aspect ratio.[4] In that study, quantitative estimates were provided for the efficiency of transfer of macroscopic strain (corresponding to that applied to the nanocomposite) to microstrain (corresponding to that observed in the clay particles).

Although it is quite straightforward to measure the macrostrain applied to a nanocomposite in the laboratory, it is relatively difficult to determine experimentally the corresponding level of microstrain imparted to the clay particles. Comparison to a micromechanical model is further complicated by the inevitable dispersity in degree of exfoliation, aspect ratio of particles, and orientation of particles. However, indirect measurements of microstrain are possible using vibrational (FTIR, Raman) spectroscopy to monitor strain at the atomic level through correlation of the shifts in the absorption peaks with deformation.[5−7] A recent FTIR study by Loo and Gleason investigated the effect of macroscopic strain on the absorbance spectrum of a nylon-6/MMT nanocomposite.[8] In particular, shifts in frequency of the 1018 and 1046 cm^{-1} peaks, corresponding to normal modes involving atoms in the clay particles, were observed upon deformation of the nanocomposite. In this way, shifts in the vibrational spectra could be correlated with the applied macroscopic strain on the nanocomposite.

Here, we report the results of molecular dynamics (MD) simulations to obtain the vibrational spectrum of a model clay as a function of strain in the clay platelet itself, i.e., microstrain. By comparing the calculated spectra obtained in the absence of applied deformation to that obtained in the presence of tensile strain along different directions in the plane of the clay platelet, we determine the spectral shifts for various states of microstrain. Eshelby's method[9] is then used to relate microstrain to macrostrain for the nanocomposite studied experimentally by Loo and Gleason, such that theoretical estimates of the spectral shifts for various states of macrostrain are obtained for comparison to that work. In this way, we seek to close the loop relating macrostrain, microstrain, and spectral shifts and to check for internal consistency. To our knowledge, these are the first available estimates of the vibrational spectra of a clay under strain.

Methods and Simulation Details

AMBER 6.0[10] was used to perform MD simulations on a model clay. The simulation box comprised 160 atoms, corresponding to four unit cells of the unsubstituted form of MMT clay, with stoichiometric formula $Si_{32}Al_{16}O_{80}(OH)_{16}$. Figure 1 shows the top view of the clay structure. The simulation cell was orthogonal, with dimensions of $x = 10.4149$, $y = 18.0289$, and $z = 9.446$ Å and periodic boundaries in all three directions. We used the recently developed CLAYFF force field, which has been shown to reproduce the bulk crystal structure of a number of different clays as well as the swelling behavior of Na−MMT and the vibrational spectrum of hydrotalcite.[11] The interatomic interactions in CLAYFF consist solely of the electrostatic and Lennard-Jones type except for the O−H bond, which is constrained by a harmonic bond stretch potential having a stiffness of 554 kcal/mol/Å^2. Lennard-Jones and

* Corresponding author. E-mail: rutledge@mit.edu.
[†] Department of Chemical Engineering.
[‡] Department of Mechanical Engineering.

10.1021/ma062144p CCC: $37.00
Published on Web 01/02/2007

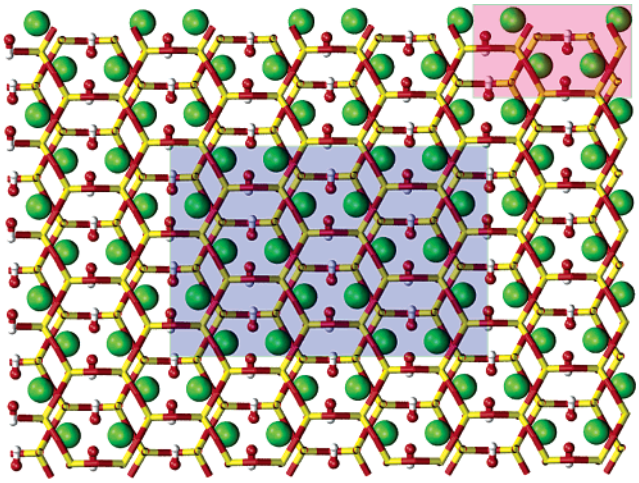

Figure 1. Top view of Montmorillonite clay with periodic boxes replicated in the two-dimensional plane ($X-Y$ direction). The simulation box is represented by blue bounding box and the unit cell by red. Aluminum atoms are shown by green spheres and silicon, oxygen, and hydrogen atoms are in yellow, red, and white wire frame representation, respectively.

Table 1. Partial Charges (q Is the Atomic Charge and e Is the Charge of an Electron) and Atom−Atom Lennard-Jones Interaction Parameters (σ and ϵ)

atom name	q/e	ϵ (kcal/mol)	σ (Å)
oxygen (bridging)	−1.05	0.1554	3.16554
oxygen (bonded to hydrogen)	−0.95	0.1554	3.16554
silicon	2.1	0.0000018405	3.30203
aluminum	1.575	0.0000013298	4.27132
hydrogen	0.425	0.0	0.0

electrostatic interaction parameters for all atoms are provided in Table 1. Canonical ensemble (constant *NVT*) simulations were performed with temperature maintained at 300 K using Berendsen's thermostat.[12] A time step of 0.1 fs was used and velocities were recorded every 10 steps for subsequent determination of the vibrational spectrum. The total simulation time was 50 ps. Long range interactions were computed using particle-mesh Ewald electrostatics in all three directions.[13] The simulation was also repeated for a box composed of 640 atoms, with dimensions of x = 20.8298 Å, y = 18.0289 Å, and z = 19.892 Å; the resulting vibrational spectrum was very similar to that obtained using the smaller box, with the exception of low-frequency modes around 100 cm^{-1}. This confirms that the effects of the 3.5 Å cutoff, as required by the minimum image convention for direct space interactions used in the smaller simulation box, are mitigated by the use of the *NVT* ensemble and do not introduce any significant error in the relevant vibrational dynamics above 800 cm^{-1}. For deformed crystals, the simulations were performed with the simulation cell dimensions increased in the x or y directions in accordance with positive strains of 2−10%; at each level of strain, data was collected for 50 ps.

The vibrational spectra were determined within the quasiharmonic approximation as the density of states obtained from the velocity spectrum:[14]

$$P^{v}(\omega) = 2\beta \sum_{j=1}^{3N} \lim_{\tau\to\infty} \frac{1}{2\tau} \left| \int_{-\tau}^{\tau} dt \exp[-i2\pi\omega t] v_j'(t) \right|^2 \qquad (1)$$

where $v_j'(t)$ is the mass-weighted velocity, $v_j'(t) = \sqrt{m_j} v_j(t)$, $v_j(t)$ is the jth component of the $3N$ velocity vector, ω is the frequency, and β is the inverse temperature:

$$\beta^{-1} = \frac{2}{3N} \lim_{\tau\to\infty} \int_{-\tau}^{\tau} dt \frac{1}{2\tau} \sum_{j=1}^{3N} \frac{1}{2} v_j'^2(t) \qquad (2)$$

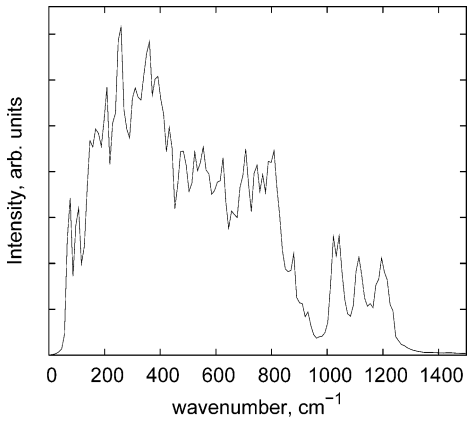

Figure 2. Vibrational spectra for unstrained clay. Solid line is a result of averaging over 20 consecutive points obtained directly from the PCA analysis at wavenumber intervals of 0.51 cm^{-1}.

We followed the formulation described by Strachan,[15] which allows decomposition of the spectrum into contributions from $3N$ normal modes by first computing the matrix $K_{ij}^{v} = \langle v_i' v_j' \rangle / 2$, i,j = 1...$3N$, constructed from the mass-weighted velocity covariances. $\langle\ \rangle$ denotes the time average. Upon diagonalization using Jacobi's method, the eigenvalues correspond to the kinetic energy of each mode, while the eigenvectors (ξ_1, ξ_2, ..., ξ_{3N}) correspond to the polarization vectors for each mode. By construction, the time evolutions of the modes thus defined are uncorrelated to each other but are not necessarily harmonic. To estimate the contribution from each mode (k), velocities of all atoms were projected onto the corresponding eigenvector by the following equation

$$v_k(t) = \sum_{j=1}^{3N} \xi_k(j) \cdot v_j'(t) \qquad (3)$$

The modal velocities in the time domain were zero-padded up to 2^{16} data points and fast-Fourier transformed according to eq 1 to yield the velocity spectrum in the range ±16667 cm^{-1} for each mode. From the relation $n\delta t\delta\omega = 1$, where n is the number of samples in the time domain, the spectral resolution was 0.67 cm^{-1}. The vibrational spectrum was finally obtained by summing the spectra over all modes.

Results

The bulk clay crystal was found to remain stable for the full duration of the simulation. The high-frequency modes associated with the OH stretching vibrations averaged out due to rotation of this group about the Si−O bond. The eigenvectors for the remaining modes were not easily assigned to specific local vibrations involving only small groups of atoms. Instead, we report in Figure 2 only the total vibrational spectrum obtained by summing over all modal densities of states. In Table 2, we summarize the correspondence between peaks in the simulated spectrum and those reported by van der Marel and Beutelspacher.[16] The root-mean-square deviation is remarkably small at 4.3 cm^{-1}. However, it must be noted that, due to the high level of noise in the spectrum, the details of the computed spectrum are somewhat sensitive to the degree of averaging performed. At low wavenumbers, in particular, the velocity spectra of different modes overlap considerably. In the 1000−1300 cm^{-1} range, however, we observe three clearly identifiable peaks at 1194, 1114, and 1042 cm^{-1}. In their experimental studies, Loo and Gleason assigned peaks at 1100, 1046, and 1018 cm^{-1} to in-plane Si−O vibration modes, while a peak at 1082 cm^{-1} was assigned to an out-of-plane Si−O vibration mode based on analyses reported by Farmer.[17]

Table 2. Comparison of Simulated and Experimental Vibration Frequencies.[a]

wavenumber (cm^{-1}) (simulation)	wavenumber (cm^{-1}) (experiment)	assignment
1195	1168[b]	Si−O
1114	1115−1090	Si−O
1042	1038−1026	Si−O−Si
932	915	Al−O−H
880	878	Al−O−H
809	845−835	Al−O−H
788	796	Al−O−H
707	695	Si−O−Al
626	623	Al−O−H
554	578[b]	Al−O−H
523	522	Si−O−Al
473	474[b]	Si−O
432	426	Si−O

[a] Experimental values and assignments from ref 16. [b] Indicates bands that only occur incidentally.

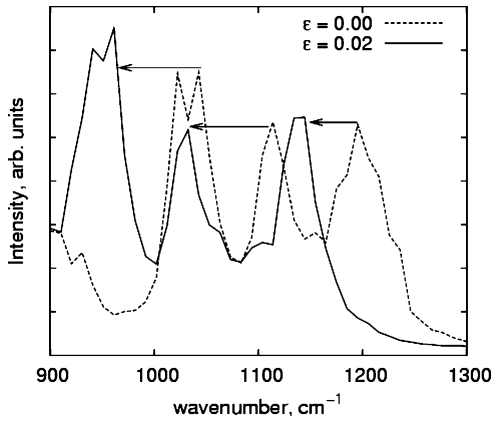

Figure 3. Vibrational spectrum of clay in the range of wave numbers between 1000 and 1300 cm^{-1}. Two sets of data are shown here: the dotted curve corresponds to unstrained clay and the solid curve to strain $\epsilon = 0.02$ in the X direction. Arrows indicate the shift in positions of the three peaks upon applying strain to the clay.

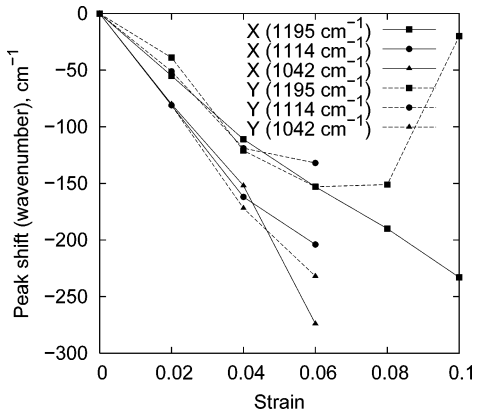

Figure 4. Changes ($\Delta\nu$) in the positions of three peaks in the 1000−1300 cm^{-1} wave number range are shown as a function of the applied strain. "X" denotes strain ϵ_{xx} from 0.02 to 0.10; "Y" denotes strain ϵ_{yy} from 0.02 to 0.10. The data are joined by straight lines as a guide to the eye.

On applying strain, we observed significant changes in the vibrational spectrum relative to that of the unstrained clay. Figure 3 shows the changes in the positions of peaks corresponding to 1194, 1114, and 1042 cm^{-1} with an applied microstrain of $\epsilon_{xx} = 0.02$. Significantly, all three peaks are shifted downward toward lower frequencies by approximately the same amount. The shapes of the three peaks are largely unaffected. Figure 4 summarizes the peak shift for the same three peaks for strains ϵ_{xx} and ϵ_{yy} up to 0.10. In all cases, the frequency shift is monotonic and toward a lower wavenumber, at least up to 6% strain. Such downward shifts with tensile strain can be explained in terms of vibrations that are dominated by short-range repulsive interactions. The shifts are relatively insensitive (with the possible exception of the 1114 cm^{-1} peak) to the direction of strain within the plane of the clay lamella. The peak shifts are grouped into one set around -29 cm^{-1}/% and another set around -40 cm^{-1}/%. Above approximately 6% strain, the peak shifts are no longer proportional to strain.

Discussion

Loo and Gleason applied tensile macrostrains of 0.005 to 0.02 (0.5 to 2%) to a UBE PA6 (polyamide 6)/Na-MMT nanocomposite in their experimental study.[8] They observed a downward shift of -1.25 cm^{-1}/% macrostrain. To account for the difference between macrostrain and microstrain, they invoked the shear lag analysis of Cox for a single, cylindrical reinforcing fiber embedded in a soft cylindrical matrix.[18] Assuming a clay loading of 1 vol %, 180 GPa for the clay modulus (corresponding to bulk mica), 0.8 GPa for the matrix modulus (corresponding to an amorphous nylon), and an aspect ratio of 1000, they estimated a maximum value of 91% strain transfer to the particle.

Before comparing our simulated results with those of Loo and Gleason, with appropriate correction for transfer of strain to the clay particle, it is necessary to account for differences in the mode of deformation. The clay particles embedded in the macroscopically tensile-loaded composite experimental samples were locally subjected to a biaxial strain state, while the deformations applied in the molecular dynamics simulations correspond to uniaxial strain with constant lateral dimension. Because our simulations indicate that the peak shift is approximately independent of direction in uniaxial strain, one would expect the peak shift in clay particles of the experimental sample to exhibit compensating strain contributions due to both extension along the loading direction and a transverse contraction. Contributions to frequency shift from out-of-plane Poisson effects are expected to be minor because three of the four vibrations in the region in question are assigned to in-plane vibrations and because out-of-plane deformation couples to both compression and extension in the plane of the clay particle, resulting in some cancellation. Assuming the in-plane effects are additive, the net shift in frequency is proportional to $\Delta\nu \sim (\epsilon_{\mathrm{micro},xx} + \epsilon_{\mathrm{micro},yy})$. Thus the observed frequency shift depends on not only the resultant microstrain $\epsilon_{\mathrm{micro},xx}$ resulting from an applied macrostrain $\epsilon_{\mathrm{macro},xx}$ but also the transverse strain resulting from Poisson effects of the particle and matrix interaction.

The method of Eshelby[9] can be used to model the uniform strain within an isolated ellipsoidal heterogeneity embedded within a linear elastic body subject to a remote strain field. Assuming the heterogeneities are sufficiently dilute that their stress fields do not interact, one can write:

$$\epsilon_{\mathrm{micro}} = \mathbf{A}\epsilon_{\mathrm{macro}} \tag{4}$$

where the inverse of the fourth-order tensor $\mathbf{A}$ connecting the remote strain tensor $\epsilon_{\mathrm{macro}}$ to the strain $\epsilon_{\mathrm{micro}}$ within the heterogeneity can be expressed as:

$$\mathbf{A}^{-1} = \mathbf{I} + \mathbf{S}:\mathbf{C}_{\mathrm{m}}{}^{-1}:(\mathbf{C}_{\mathrm{p}} - \mathbf{C}_{\mathrm{m}}) \tag{5}$$

Here $\mathbf{C}_p$ is the elastic stiffness tensor of the particle (heterogeneity), $\mathbf{C}_m$ is the stiffness tensor of the matrix material, and its inverse, $\mathbf{C}_m^{-1}$, is the compliance tensor, and $\mathbf{I}$ is the fourth-order identity tensor. $\mathbf{S}$ is the dimensionless Eshelby tensor, which, for an isotropic linear elastic matrix, depends on only the matrix Poisson ratio, ν_m, and the particle aspect ratio, L/h; details can be found in Mura[19] and Kachanov et al.[20]

To first order,[20] the composite stiffness tensor can be obtained as a function of particle volume fraction, f, using:

$$\mathbf{C}_{composite} = \mathbf{C}_m + f(\mathbf{C}_p - \mathbf{C}_m):\mathbf{A} \qquad (6)$$

Manevitch and Rutledge[21] have previously reported theoretical values for the elastic properties of a single lamella of unsubstituted MMT clay. They argued that the primary material property for a single lamella with thickness of atomic dimensions is the membrane modulus Eh, with units N/m rather than N/m^2, and reported a value of about 255 N/m for MMT. For purposes of most composite models, modulus E and lamellar thickness h must be specified separately, but any choice of lamellar thickness results in compensatory effects on particle modulus and volume fraction (whose conversion from weight fraction also depends on h). Moreover, within the Eshelby formalism, a third dependency on assigned thickness appears in the aspect ratio dependence of the tensor $\mathbf{S}$. To illustrate this, we assumed three different values of lamellar thickness, listed in decreasing scale: a nominal value of $h = 1$ nm, an intermediate $h = 0.823$ nm, consistent with the density of clay reported by Loo and Gleason,[8] and $h = 0.625$ nm, the average distance reported by Manevitch and Rutledge[21] between opposing layers of oxygen atoms centers at each surface of the sheet. For these thicknesses, the corresponding particle moduli are 255, 310, and 408 GPa, respectively, and the corresponding volume fractions are $f = 0.020$, 0.017, and 0.13, respectively, consistent with 5 wt % exfoliated clay. In addition, we take $\nu_p = 0.45$[21] and $E_m = 0.5$ GPa, in accord with the measurement of films made from the unmodified UBE PA6 by Loo and Gleason,[22] and $\nu_m = 0.4$. The particle length (diameter) is assumed to be 100 nm, and all particles are assumed to be oriented with their normal direction perpendicular to the plane of the film. Using eqs 5 and 6, the calculated composite in-plane tensile moduli are 1.124, 1.122, and 1.120 GPa for the three thickness cases, respectively. The small (0.3% maximum) difference among these estimates is indicative of the strongly compensatory effects of modulus, aspect ratio, and volume fraction for different choices of lamellar thickness. A more significant difference arising from alternate choices of lamellar thickness could show up in bending deformation of the lamella, but according to the Eshelby analysis, an isolated ellipsoid in the presence of a homogeneous strain field adopts a homogeneous state of strain, and does not bend. Furthermore, these theoretical estimates for the composite modulus are in reasonable agreement with the experimentally determined composite modulus of 1.2 GPa[23] and lend credence to our use of Eshelby's method in this case. For the case of $h = 0.625$ nm, on using the value of $(\mathbf{C}_{composite})^{-1}$ predicted by the Eshelby analysis, we estimate the ratio of strain at the macroscopic level to be $\epsilon_{macro,xx}:\epsilon_{macro,yy}:\epsilon_{macro,zz} = 1.0:-0.291:-0.473$, with similar ratios inferred for the other thicknesses. In turn, using eq 4 to compute microstrain for each case, we obtain strain transfer efficiencies $(\epsilon_{micro,xx} + \epsilon_{micro,yy})/\epsilon_{macro,xx}$ of 0.0562, 0.0559, and 0.0557, respectively, for the three thickness cases. The results of the Eshelby analysis were also compared to more detailed three-dimensional micromechanical modeling based on that of Sheng et al.[4] and found to be consistent with those as well.

Finally, we correct the simulated spectral shifts of -29 to -40 cm^{-1}/% microstrain using the calculated particle/composite strain transfer efficiency of 5.6% to obtain a theoretical shift estimate of -1.6 to -2.2 cm^{-1}/% macrostrain. This agrees reasonably well with the experimentally measured value of -1.25 cm^{-1}/% macrostrain obtained by Loo and Gleason and suggests that the theoretical calculations adequately capture the primary features of deformation in the nanocomposite.

For completeness, we consider some remaining possible sources of discrepancy arising both from the atomistic modeling of the clay and from the adopted micromechanical model of the nanocomposite. The former include inaccuracies in the force field, interactions between adjacent clay lamellae in the bulk-phase simulation that are not present in the exfoliated clay−polymer nanocomposite and vice versa, and differences in the chemical compositions of the simulated and experimental clays, while the latter include some uncertainty in assumed material parameters and the misalignment of the particles with respect to the in-plane deformation directions. Each of these is considered in turn.

The good agreement with experiment for vibrational frequencies of hydrotalcite reported by Cygan et al.,[11] as well as those for MMT reported here, suggest that errors in the force field and differences in the chemical composition of the model clay from the common form of MMT are probably insignificant, or at least compensatory, for the vibrational modes of interest here. The good agreement between the relevant normal mode vibration frequencies for the clay component of the nanocomposite and those reported for bulk clay (cf. ref 16) indicates that differences between platelet−polymer and platelet−platelet interactions are also probably not significant sources of error.

Other possible sources of uncertainty that would affect the micromechanical modeling include diameter of the clay particles, degree of exfoliation (which affects not only the aspect ratio but also the effective particle modulus and estimated clay volume fraction[4]), and morphological differences in the PA6 matrix that might affect the 0.5 GPa estimate for the matrix modulus; we believe this relatively low matrix modulus value may be due to plasticization by water of the thin, 5−7 μm films studied by Loo and Gleason, despite efforts to minimize contact with the atmosphere. The PA6 matrix is also semicrystalline, with varying contents of α- and γ-crystallites, depending on sample history. Another source of error in the micromechanical modeling is that due to particle misalignment. Using FTIR and transmission electron microscopy, Loo and Gleason have estimated that the angular deviation between the film normal and the normals to the clay particles in their samples is well-described by a Gaussian distribution having a standard deviation of 15°.[24] To assess the significance of this, we used an orthogonal rotation tensor $\mathbf{R}$ to calculate a rotated macroscopic strain tensor $\epsilon_{macro}^{(rot)} \equiv \mathbf{R}\epsilon_{macro}\mathbf{R}^T$ for rotations up to 30° (i.e., two standard deviations) from the axis of deformation and inserted this into eq 4. For 0°, 15°, and 30° particle rotations, the strain transfer efficiency decreases from 0.056 to 0.048 for 15° and 0.027 for 30°. The effects of particle misalignment corresponding to rotations of such magnitude about the tensile direction are substantially less and have precisely zero effect when the $\epsilon_{macro,yy} = \epsilon_{macro,zz}$. These modest sensitivities of calculated particle strain to misorientation would tend to diminish the magnitude of predicted downward shifts per unit macrostrain, actually bringing the theoretical calculations into better agreement with the experiments.

Conclusions

The foregoing analysis allows for a reconciliation of recent experimental results and micromechanical modeling of the deformation of the clay component in a nanocomposite. Using vibrational data to relate macrostrain to frequency shifts in the clay vibration spectrum, Eshelby's analysis to relate macrostrain to microstrain in the clay particles themselves, and molecular dynamics modeling to relate microstrain to frequency shifts in the clay vibration spectrum, a consistency check for the three methods can be performed that involves no adjustable parameters. The theoretical estimate of -1.6 to -2.2 $cm^{-1}/\%$ macrostrain is in reasonable accord with the experimentally measured value of -1.25 $cm^{-1}/\%$, and the theoretical modulus of 1.12 GPa for the composite is also in good accord with the experimentally measured value of 1.2 GPa. We believe this analysis provides compelling support for the accuracy of the methods involved.

Acknowledgment. We thank N. Sheng, L. Loo, and K. K. Gleason for substantial discussions regarding the analysis presented here. We also gratefully acknowledge financial assistance provided by the DURINT on Microstructure, Processing, and Mechanical Performance of Polymer Nanocomposites, Air Force contract no. F49620-01-1-0447.

References and Notes

(1) Messersmith, P. B.; Giannelis, E. P. *Chem. Mater.* **1994**, *6*, 1719.
(2) Kojima, Y.; Usuki, A.; Kawasumi, M.; Okada, A.; Fukushima, Y.; Kurauchi, T.; Kamigaito, O. *J. Mater. Res.* **1993**, *8*, 1185.
(3) Ray, S. S.; Okamoto, M. *Prog. Polym. Sci.* **2003**, *28*, 1539.
(4) Sheng, N.; Boyce, M. C.; Parks, D. M.; Rutledge, G. C.; Abes, J. I.; Cohen, R. E. *Polymer* **2004**, *45*, 487.
(5) Robinson, I. M.; Young, R. J.; Galiotis, C.; Batchelder, D. N. *J. Mater. Sci.* **1987**, *22*, 3642.
(6) Tashiro, K.; Minami, S.; Wu, G.; Kobayashi, M. *J. Polym. Sci. Phys.* **1992**, *30*, 1143.
(7) Andrews, M. C.; Bannister, D. J.; Young, R. J. *J. Mater. Sci.* **1996**, *31*, 3893.
(8) Loo, L. S.; Gleason, K. K. *Macromolecules* **2003**, *36*, 2587.
(9) Eshelby, J. D. *Proc. R. Soc. London, Ser. A* **1957**, *241*, 376.
(10) Pearlman, D. A.; Case, D. A.; Caldwell, J. W.; Ross, W. S.; Cheatham, T. E.; Debolt, S.; Ferguson, D.; Seibel, G.; Kollman, P. *Comput. Phys. Commun.* **1995**, *91*, 1.
(11) Cygan, R. T.; Liang, J. J.; Kalinichev, A. G. *J. Phys. Chem. B* **2004**, *108*, 1255.
(12) Berendsen, H. J. C.; Postma, J. P. M.; van Gunsteren, W. F.; DiNola, A.; Haak, J. R. *J. Chem. Phys.* **1984**, *81*, 3684.
(13) Darden, T.; York, D.; Pedersen, L. *J. Chem. Phys.* **1993**, *98*, 10089.
(14) Berens, P. H.; Mackay, D. H. J.; White, G. M.; Wilson, K. R. *J. Chem. Phys.* **1983**, *79*, 2375.
(15) Strachan, A. J. *Chem. Phys.* **2004**, *120*, 1.
(16) Van der Marel, H. W.; Beutelspacher, H. *Atlas of Infrared Spectroscopy of Clay Minerals and their Admixtures*, Elsevier: New York, 1976.
(17) Farmer, V. C.; Russell, J. D. *Spectroschim. Acta* **1964**, *20*, 1149.
(18) Cox, H. L. *Br. J. Appl. Phys.* **1952**, *3*, 72.
(19) Mura, T. *Micromechanics of Defects in Solids*, 2nd ed.; Martinus Nijhoff: Dordrecht, The Netherlands, 1987.
(20) Kachanov, M.; Shafiro, B.; Tsukrov, I. *Handbook of Elasticity Solutions*; Springer: Berlin, 2003.
(21) Manevitch, O. L.; Rutledge, G. C. *J. Phys. Chem. B* **2004**, *108*, 1428.
(22) Loo, L. S.; Gleason, K. K. *Macromolecules* **2003**, *36*, 6114.
(23) Loo, L. S., private communication.
(24) Loo, L. S.; Gleason, K. K. *Polymer* **2004**, *45*, 5933.

MA062144P